
Shinji YOSHIDA

An evaluation of the effects of heat ray retro-reflective film on the outdoor thermal environment using a radiant analysis method

Shinji YOSHIDA[1], Saori YUMINO[2], Akashi MOCHIDA[3], Taiki UCHIDA[4]

[1] *University of Fukui, 3-9-1 Bunkyo, Fukui-city, Fukui, Japan, y-shinji@u-fukui.ac.jp*

2 Tohoku University, 6 Aoba, Sendai, Miyagi, Japan, yumino@sabine.pln.archi.tohoku.ac.jp

3 Tohoku University, 6 Aoba, Sendai, Miyagi, Japan, mochida@sabine.pln.archi.tohoku.ac.jp

4 Tohoku University, 6 Aoba, Sendai, Miyagi, Japan, taiki@sabine.pln.archi.tohoku.ac.jp

1. Introduction

In recent years, low-e double glazing and heat-shading films for windows have been widely adopted to reduce building cooling loads in the summer. However, these windows usually reflect solar radiation towards pedestrian spaces. Hence, these modifications have a negative impact on the thermal comfort of pedestrians. As a countermeasure to this problem, we consider a heat ray retro-reflective film for application to windows (Fujita et al 2014). It is expected that the use of this film will achieve positive effects by reducing the indoor cooling load while mitigating effects on the thermal environment in outdoor spaces near the ground, where pedestrians come and go, as shown in Fig. 1.

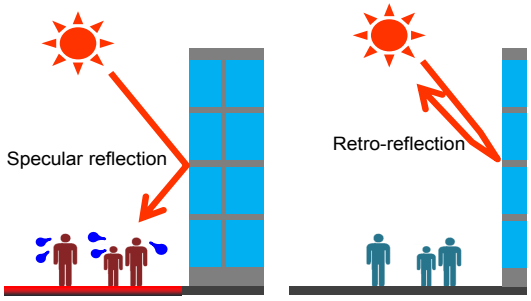

Fig. 1 Effect of adopting a retro-reflective film on thermal environment in outdoor space in summer season.

Recently, some Japanese researchers, including the present authors, have been studying the thermal environment in urban and building spaces and have developed computational methods for analysing the radiant environment in outdoor spaces (e.g., Yoshida et al. 2006). These computational methods enable us to estimate the three-dimensional distributions of incident short- and long-wave radiation on pedestrians at any location in the computational domain and evaluate the effects of the radiation on the thermal comfort of pedestrians. However, in most of these analyses, each surface in the computational domain is assumed to be a perfectly diffuse (or Lambertian) surface. Therefore, most of the existing methods used for radiant analysis do not allow us to evaluate the effects of a heat ray retro-reflective film for windows on the thermal environment in urban and building spaces.

In this study, we incorporated the effects of the directional reflectivity of surfaces into the existing computational method, and evaluated the effect of a window with a heat ray retro-reflective film on the thermal environment of an outdoor space.

2. Outline of revised method for radiant computation

2.1 Definition of elevation and azimuth angles

Figure 2 illustrates the local coordinate system for a surface element *i* that was used to define elevation and an azimuth angles in this study. The elevation angle θ was defined as the angle between the normal line to the surface element *i* and the incident or reflective heat ray. Hence, $\theta = 0°$ is normal to *i*, while $\theta = 90°$ is tangent to *i*. The azimuth angle φ was defined as the angle between the X-axis in the local coordinate system and the incident/reflective heat ray, with counterclockwise rotation angles taken to be positive. In the field of building environmental engineering, the angle for which rotation is clockwise is defined as the azimuth A_z, as shown in Fig. 2. However, in mathematical coordinates, the former angle (φ) is more readily applied. Thus, both definitions are used in this paper.

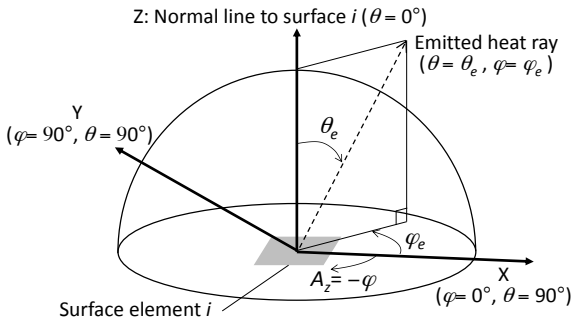

Fig.2 Definition of an elevation and an azimuth angle in a local coordinate system on a surface element i.

2.1 Existing method for radiant computation

Radiosity, or the total radiation energy flux leaving a surface per unit area and unit time, is defined as shown in Eq. (1):

$$R_i = E_i + \rho_i \sum_{j=1}^{N} F_{ji} R_j, \quad (1)$$

where R_i is the radiosity [W], ρ_i is the reflectance of the surface element *i*, E_i is the radiation emitted at the surface

element i [W], and F_{ij} is the form factor, i.e., the fraction of radiation leaving the surface element i that is intercepted by a surface element j. In this method, each surface in the computational domain is assumed to be a perfectly diffusively reflecting (or Lambertian) surface. Therefore, the radiosity of surface element i that is intercepted by a surface element j per unit of solid angle $R_{i(j)}$ is defined by the following equation:

$$R_{i(j)} = R_i/\pi. \quad (2)$$

As Eq. (2) shows, most of the existing methods cannot evaluate the radiant field that is strongly affected by directional reflection, such as the radiant field around a window with a heat ray retro-reflective film.

2.2 Equations for radiant computation considering directional reflection

In this study, to consider the effect of directional reflection, radiant heat exchanges between urban surfaces were calculated using a method proposed by Yoshida et al. (2014). This method is a revised version of the progressive radiosity method extended to directional radiant computation (Ichinose et al. 2005) for outdoor spaces.

The equations for the expanded radiosity method are as follows:

$$R_{i(j)} = E_{i(j)} + \sum_{k=1}^{N} \kappa_{ki} F_{ki} \cdot \rho_{ki(j)} \cdot \pi \cdot R_{k(i)} \quad (3)$$

and $$\kappa_{ki} = \rho_{hemi(k,i)} / \sum_{j=1}^{N} F_{ij} \cdot \pi \cdot \rho_{ki(j)}, \quad (4)$$

where $R_{i(j)}$ is the radiosity per unit solid angle of surface element i intercepted by surface element j [W/sr], $E_{i(j)}$ is the radiation per unit solid angle emitted from surface i to surface j [W/sr], $\rho_{ki(j)}$ is the fraction of the radiosity reaching surface j from surface k via surface i per unit solid angle [1/sr], κ_{ki} is the correction coefficient of the distribution of the reflected radiosity from surface k to surface i, and $\rho_{hemi(k,i)}$ is the reflectivity measurement value from surface k via surface i to the surroundings.

In this study, we incorporated this method into the analysis of spatial distributions of solar radiation. In this case, $E_{i(j)}$ is the sum of the reflective components of incident, direct, and diffusive solar radiation at surfaces i to j:

$$E_{i(j)} = \rho_{(\theta_S,\varphi_S;\, i,j)} E_{Di} + \sum_{k=1}^{N_{sky}} \kappa_{ki} \rho_{ki(j)} A_i F_{ik} I_{SH}, \quad (5)$$

where θ_S and φ_S are the elevation and the azimuth angles of the sun's ray to the plane, respectively; E_{Di} is the direct solar radiation gain to surface i [W]; N_{sky} is the number of surface elements that comprise the sky area; A_i is the area of surface i; and I_{SH} is the incident sky solar radiation on a horizontal surface [W/m^2].

In the method described here, the distributions of the directional reflectivity per unit solid angle $\rho_{i,j(k)}$ affect the calculation results considerably. Ichinose et al. (2005) set the value of $\rho_{i,j(k)}$ using the anisotropic body of rotation of the normal distribution function (AND) model that was proposed by Makino et al. (1999). In this study, we adopted the AND model for the calculation of $\rho_{i,j(k)}$ for the heat ray retro-reflective film applied to windows. For the details of the calculation method, refer to Yoshida et al. (2015).

3. Outline of the analysis

3.1 Study area

Figure 3 illustrates the computational domain considered in the analysis. It was assumed that a building stands in a domain where no effects of complex terrain and other building locations need be considered. We made this assumption because we intended to obtain simple calculation results for evaluating only the effect of a heat ray retro-reflective film on the thermal environment of an outdoor space. The window was assumed to be installed on the western surface of the building, and the window ratio was set to 80%. In this analysis, we evaluated differences in the radiant environment due to changes in the window properties on this surface.

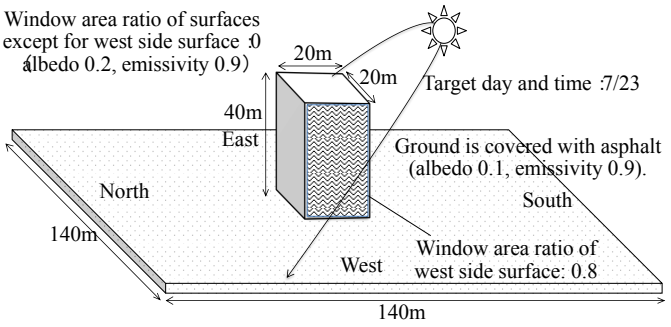

Fig. 3 Computational domain in the present analysis.

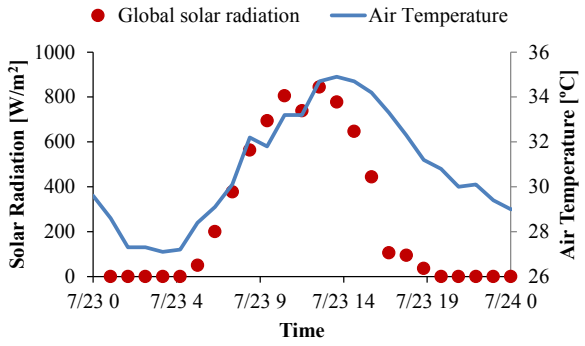

Fig. 4 Time variations of global solar radiation and air temperature.

Table 1. Meteorological condition at the target time for this analysis

Target time	14:00 on 23rd July in 2010
Weather	A particular hot summer day
Global solar radiation [W/m^2]	777.8
Sun's altitude [deg]	57.1
Sun's azimuth [deg]	71.1 (nearly WSW)
Air temperature [°C]	34.9
Relative humidity [%]	49
Wind direction and velocity	SSE, 1.2m/s

3.2 Meteorological conditions

We investigated the thermal environment for a particularly hot summer day. Meteorological data measured at the Japan Meteorological Agency in Tokyo were used in this study, and the target date was set to the 23rd of July in 2010. The start of the analysis period was 06:00 on the day before the target date, and a time integration of 48 hours was performed using the meteorological data. The thermal environment for a pedestrian was evaluated using the results obtained at 14:00 on the target date, as described later. Figure 4 illustrates the temporal variations in the global solar radiation and local air temperature during the analysis period, as examples of the meteorological data used. Table 1 also summarises the meteorological conditions at the target time used for the evaluation of outdoor thermal comfort for the pedestrian.

3.3 Computational cases

In this study, the following two computational cases were investigated. In Case 1, it was assumed that single-float glass with a heat-shading film (HSF) was used for the western window of the building, while single-float glass with a heat ray retro-reflective film (RRF) was used in Case 2. We modelled the radiant properties of these windows using the AND model in accordance with experimental results for each window.

4. Results and discussion

4.1 Performance of each window in reflecting solar radiation

Figure 5 illustrates distributions of absorptance, transmissivity, and specular and retro reflectance for each case, with respect to the incident elevation angle, calculated using the AND model. The experimental measurement data for Case 2 are also shown in this figure. We can see that there is a relatively wide variation in the values for Case 2. The reason for this is that the incident azimuth and incident elevation angle both affect the radiant properties of the window with the heat ray retro-reflective film, while those of the other window are only affected by the incident elevation angle.

Figure 6 illustrates the time variations of the solar reflectivity of the retro-reflective window that faces the western direction. The sun moves from the south to the west during the period from around noon to approximately 16:00. The incident angle of the solar radiation to the surface decreases dramatically with the change in the position of the sun. This dramatic decrease in the incident angle causes a decrease in the specular reflectivity. The value of the retro-reflectivity reaches approximately 0.2 at approximately 14:00. This value is approximately twice as much as the value of the specular reflectivity at that time. It was expected that the effects of retro-reflection would be most prominently evident at that time. For these reasons, we evaluated the effect that the heat ray retro-reflective film had at 14:00.

4.2 Effects of installed windows on specular and retro reflectivity

The reflectivity of the solar radiation at the western window for Case 1 at 14:00 is compared with that for Case 2 in Fig. 7. The sun's altitude, the sun's azimuth, and the incident angle of the solar radiation to the window at this time were approximately 71.1°, 57.1°, and 59.1°, respectively. For Case 1, the solar reflectivity was approximately 0.29, while that for

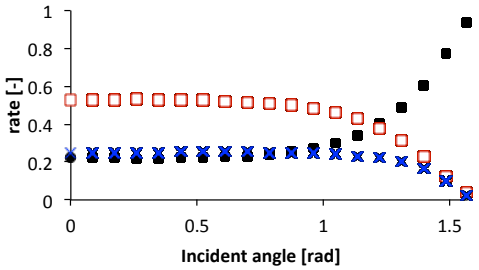

(1) Case 1
(Single float glass with heat shading film, AND model)

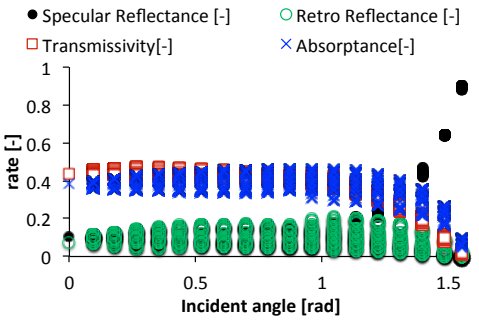

(2) Case 2
(Single float glass with heat ray retro-reflective film, AND model)

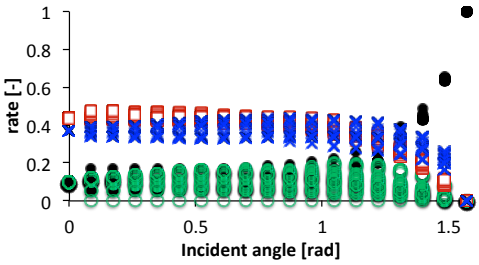

(3) Case 2
(Single float glass with heat ray retro-reflective film, measurement data)

Fig.5 Distributions of absorptance, reflectance, transmissivity on each incident elevation angle to window

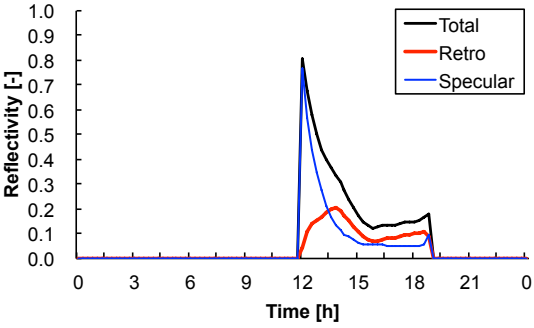

Fig. 6 Time variations of total, retro, and specular reflectivity of the retro-reflective window facing the western direction on July 23rd.

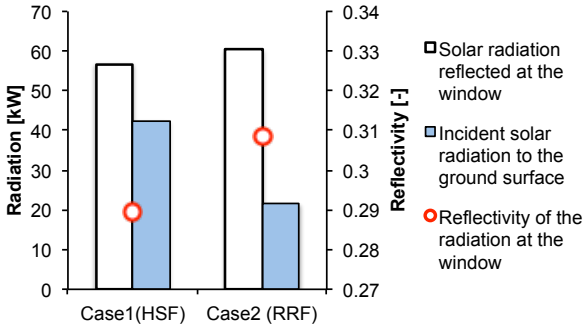

Fig. 7 Solar radiant reflectivity on window, and heat budget between window and ground surface.

Case 2 was approximately 0.31. These values correspond well to the values extracted from Figs. 5 and 6.

Figure 7 also illustrates a relationship between the solar radiation reflected at the western window of the building and the incident radiation to the ground surface near the west side of the building after being reflected at the window. For both cases, the radiation reflected at the window was approximately 60 kW. For Case 1, the incident radiation to the ground after reflection was approximately 40 kW, while for Case 2, it was approximately 20 kW. Hence, it is estimated that approximately 67% of the radiation reflected at the window re-enters the ground surface in Case 1, while only approximately 33% does so in Case 2. Our computational method includes consideration of the sky radiation, or the diffusive radiation, which reflects homogeneously at the incident to surface elements in the computational domain. In Case 1, approximately 33% of the reflected radiation returns to the sky, while in Case 2, approximately 67% of the radiation also returns to the sky, because of the effect of the retro-reflective film. Thus, it is estimated that the amount of radiation reflected to the sky in Case 2 is equivalent to twice the radiation reflected in Case 1.

4.3 Distributions of absorbed solar radiation at the ground surface

Figure 8 shows the distributions of absorbed solar radiation at the ground surface and the distributions of the difference in absorbed solar radiation for the two cases. In both cases, there are large differences in the absorbed solar radiation between a sunny area and a shaded area. In Case 1, the values near the western window are approximately 800 W/m^2, while those in Case 2 approximately 725 W/m^2. The values near the window are considerably larger than those near the surrounding ground surfaces. These differences are caused by the

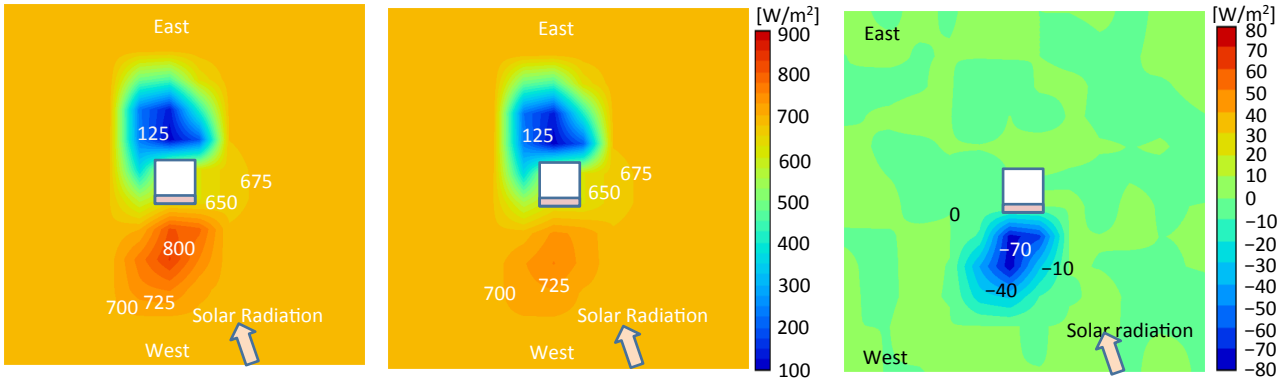

(1) Case 1 (HSF) *(2) Case 2 (RRF)* *(3) Case 2 – Case 1*

Fig. 8 Distributions of absorbed solar radiation and difference between Case2 (Retro- Reflective Film) and Case 1 (Heat-Shading Film) at 14:00 on July 23rd.

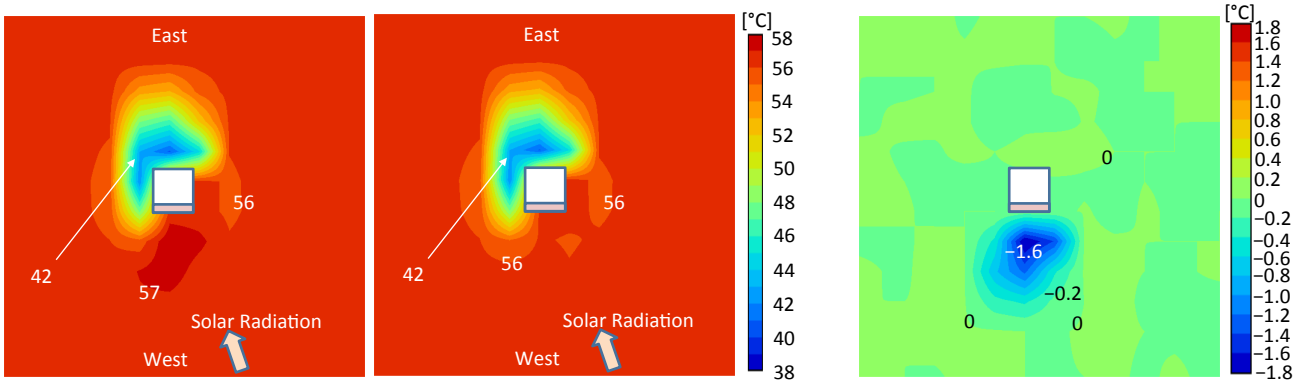

(1) Case 1 (H. S. F.) *(2) Case 2 (R. R. F.)* *(3) Case 2 – Case 1*

Fig. 9 Distributions of ground surface temperature and difference between Case2 (Retro- Reflective Film) and Case 1 (Heat-Shading Film) at 14:00 on July 23rd.

(1) Incident solar radiation *(2) MRT*

Fig. 10 Azimuthal distributions of solar radiation and MRT for the entire body of a pedestrian facing each direction at 14:00 on July 23rd.

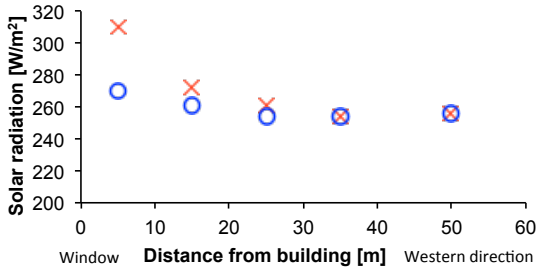

(1) Incident solar radiation

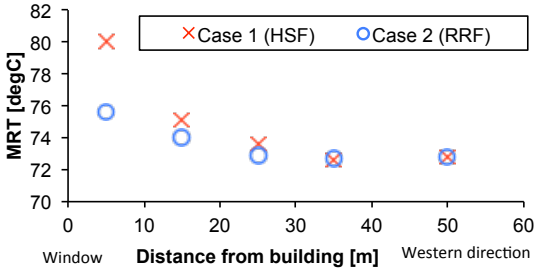

(2) MRT

Fig. 11 Comparisons of incident solar radiation and MRT for the entire body of a pedestrian between Case 1 and Case 2 at 14:00 on July 23rd.

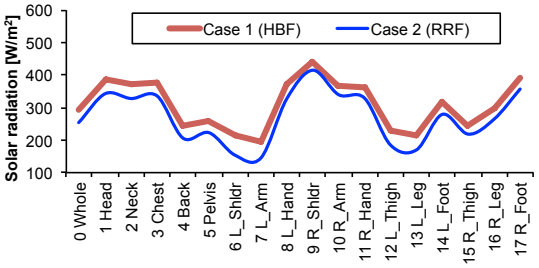

(1) Orientation of a pedestrian is 0° (South)

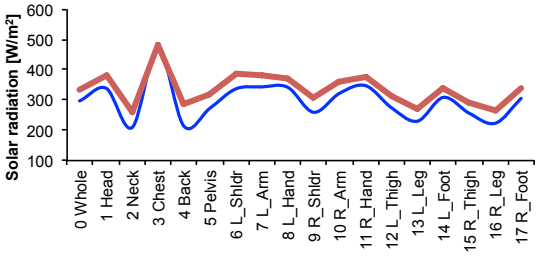

(2) Orientation of a pedestrian is 90° (West)

Fig. 12 Distributions of incident solar radiation on each body segment for the pedestrian

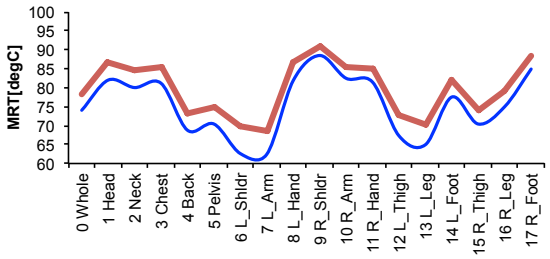

(1) Orientation of a pedestrian is 0° (South)

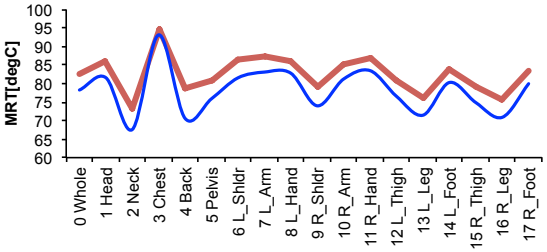

(2) Orientation of the pedestrian is 90° (West)

Fig. 13 Distributions of MRT on each body segment for the pedestrian

incident radiation from the window after reflection. Focusing on the difference between the two cases, the absorbed solar radiation around the west surface of the building in Case 1 was greater than that in Case 2 by up to approximately 70 W/m^2 because of the reduction of the specular reflection component of solar radiation resulting from the use of the heat ray retro-reflective film.

4.4 Distributions of ground surface temperature

Figure 9 illustrates the distributions of the ground surface temperature and the distributions of the difference in ground surface temperature for the two cases. The trends of the distributions and that of the difference are similar to those for the absorbed solar radiation on the ground surface, shown in Fig. 8. The difference in the temperature around the west surface of the building in Case 1 was greater than that in Case 2 by up to approximately 1.6°C.

4.5 Investigation of radiant thermal environment for a pedestrian

Figure 10 illustrates azimuthal distributions of the incident solar radiation and the mean radiant temperature (MRT) for the entire body of a pedestrian. The values shown in Figs. 10, 11, 12, and 13 were calculated using the method for analysing inhomogeneous radiant environments proposed by Yoshida et al. (2014). In this figure, it is assumed that the pedestrian is standing near the western surface of the building. We calculated 24 incident solar radiation or MRT values, where the pedestrian orientation differed by 15° between each value. In the results for both the radiation and the MRT, values from 75° (southwest) of the azimuth to 90° (west) and those from -105° (northeast) to -90° (east) were relatively large. At these orientations, the solar radiation irradiates the pedestrian from the front side or the back side direction. In Case 1, the value of the incident solar radiation at 75° of azimuth is also approximately 340 W/m^2, while that at the diagonal orientation, or -105°, is approximately 310 W/m^2. Hence, the value in the case of solar radiation irradiating from the front orientation side is slightly larger than that in the case of solar radiation irradiating from the back side direction. The values for Case 2 are approximately 50 W/m^2 of solar radiation and approximately 5°C of MRT smaller than those for Case 1.

Figure 11 illustrates the distributions of the incident solar radiation and MRT for the entire body of a pedestrian plotted with respect to distance to the west from the window of the building. The values in the figure are averages of the 24 incident solar radiation or MRT values shown in Fig. 10. The values of the incident solar radiation to a pedestrian in Case 2 are approximately 40 W/m^2 smaller than those in Case 1. These differences result from the

fact that the window with the retro-reflective film in Case 2 returns more than half of the radiation reflected to the sky. The values of MRT for Case 2 are also approximately 5°C smaller than those for Case 1 as the incident solar radiation decreases.

Figure 12 shows the incident solar radiation to each body segment of a pedestrian. Figure 13 also shows the distributions of MRT on each of these segments. The orientation of the pedestrian was set to the southern direction to obtain the results shown in Fig. 12 and to the western direction to obtain the results shown in Fig. 13. At an orientation of 0°, the maximum difference in the absorbed solar radiation between the two cases appeared at the left shoulder (6 L_Shldr). The amount of solar radiation absorbed by the left shoulder in Case 2 decreased by approximately 60 W/m^2, and the partial MRT at the same segment decreased by approximately 7.0°C. At an orientation of 90°, the maximum difference in the absorbed solar radiation between the two cases appeared at the back segment (4 Back). The amount of solar radiation absorbed by the left shoulder in Case 2 decreased by approximately 75 W/m^2, and the partial MRT at the same segment in Case 2 decreased by approximately 8.2 °C.

Table of symbols

A_i	Area of surface *i*	W
E_{Di}	Direct solar radiation gain to surface *i*	W
E_i	Radiation emitted at the surface element *i*	W
$E_{i(j)}$	radiation per unit solid angle emitted from surface *i* to surface *j*	W/sr
F_{ij}	Form factor for a surface element *i* to a surface element *j*	-
I_{SH}	Incident sky solar radiation on a horizontal surface	W/m^2
N_{sky}	Number of surface elements that comprise the sky area	-
R_i	Radiosity at the surface element *i*	W
$R_{i(j)}$	Radiosity of surface element *i* intercepted by a surface element *j* per unit of solid angle	W/sr
θ	Elevation angle	rad
θ_i	Incident elevation angle to the plane	rad
θ_o	Reflect elevation angle to the plane	rad
θ_S	elevation angle of the sun's rays to the plane	rad
κ_{ki}	Reflectance of the surface element *i*	-
$\rho(\theta_i; \theta_o; \varphi_o)$	Total directional reflectivity per unit solid angle at the incident elevation angle θ_i, the reflect elevation angle θ_o, and the reflect azimuth angle φ_o	1/sr
$\rho_{hemi(k, i)}$	reflectivity measurement value from surface *k* via surface *i* to the surroundings	-
ρ_i	Reflectance of the surface element *i*	-
ρ_{kij}	fraction of the radiosity reaching surface *j* from surface *k* via surface *i* per unit solid angle	1/sr
σ	representative value for the peak width of $\rho_S \cos\theta_o$	m
φ	Azimuth angle	rad
φ_o	Reflect azimuth angle to the plane	rad
φ_S	Azimuth angle of the sun's rays to the plane	rad

5. Conclusions

The effect of a heat ray-retro reflective film on the thermal environment in an outdoor space was evaluated using a numerical simulation based on the radiant analysis method with consideration of directional reflection.

In the present analysis, the radiant environment around a single building was simulated for two different glazing types applied to a window surface. The analysis of the results showed that (1) the amount of radiation reflected to the sky using a single-float glass window with heat ray retro-reflective film was equivalent to twice the radiation reflected using a single float glass window with heat shading film, and (2) the MRT around the retro-reflective window was lower by up to 5°C than that around the heat-shading window.

In future research, the thermal environment of a real town block will be simulated based on the application of heat ray retro-reflective film, and the effects of the heat ray retro-reflective film will be evaluated.

Acknowledgment

This work was supported by JSPS Grant-in-Aid for Scientific Research (B) (Grant Number 26289200) and Grant-in-Aid for JSPS Fellows.

References

Fujita, S., Inoue, T., Ichinose, M., Nagahama, T., and Takakusa, S., 2014: Improvement of outdoor radiative environment by high-reflective façade, *J. Environ. Eng*., *AIJ*, **79**, 696, 167-172 (in Japanese with English abstract).

Ichinose, M., Ishino, H., Kohri, K., and Nagata., A., 2005: Calculation method of radiant heat transfer with directional characteristics, *Technical papers of annual metting of IBPSA-Japan* (in Japanese with English abstract).

Makino, T., Nakamura, A., and Wakabayashi., H., 1999: Directional characteristics of radiation reflection on rough metal surfaces with description of heat transfer parameters, *The Japan society of mechanical engineering*, B, **65**, 630: 324-330 (in Japanese with English abstract).

Yoshida, S., Ooka, R., Mochida, A., Murakami, S., and Tominaga, Y., 2006: Development of three dimensional plant canopy model for numerical simulation of outdoor thermal environment, *In Proceedings of the 6th International Conference on Urban Climate (ICUC6)*, 320-24.

Yoshida, S., Sato, T., and Oguro, M., 2014: Study on Evaluation of Effects of Inhomogeneous Radiant Environment for Pedestrian in Summer Season using a Coupled Numerical Simulation based on CFD Analysis, *In Proceedings of 8th Windsor Conference*, W14064.

Yoshida, S., Yumino, S., Uchida, T., and Mochida, A., 2015: Effects of windows with heat ray retro-reflective film on outdoor thermal environment and building cooling load, *Journal of heat island institute international*, 9-2, 67-72.